

---

---

# THE INHERENT STRAIN METHOD FOR RESIDUAL STRESS DETERMINATION AND ITS APPLICATION TO A LONG WELDED JOINT

**Michael R. Hill**  
**Drew V. Nelson**  
Mechanical Engineering Department  
Stanford University  
Stanford, CA

## ABSTRACT

In this paper, we investigate a relatively new method for determining three-dimensional sub-surface residual stress (Ueda, 1975). This hybrid experimental/analytical method determines the source of residual stress by sectioning and strain measurement, and then uses it to deduce residual stress in the original body. When certain assumptions about the spatial distribution of the source of residual stress can be made, estimates of residual stress can be generated for locations which are remote from strain measurement points. We outline the method and then illustrate its application to measurement of residual stress in a long welded joint. First, background regarding the nature of residual stress and a formulation of the inherent strain approach to residual stress determination is discussed. Then, application of this method to a long continuously welded joint is described. A model problem is developed and solved by application of finite element analysis. Taking the finite element stress results as if they were experimental measurements, the inherent strain method is used to find residual stress. The accuracy of the method is then investigated by comparing the inherent strain and finite element solutions. Finally, the advantages and drawbacks of this relatively new method are discussed.

## INTRODUCTION

### Description of the inherent strain method for residual stress determination

The source of residual stress in a body is an incompatible strain field. By incompatible, we mean that the strain field cannot exist within the body without stress. Stress must be present so that the strain field will fit within the body. Thinking of this as a mechanical operation, the body must be

deformed to fit the strain field in. Then loads required to deform the body are removed and equilibrium found to obtain the residual stress state. The ill-fitting strain field could be produced by plastic deformation, thermal strain, phase-transformation, or other means. Ueda (1975) refers to the sum total of all such possible causes of incompatible strain as the “inherent strain” present in the body. Any stress present in the unloaded body is then a result of the strain which does not fit, the inherent strain.

When a body contains residual stress, cutting the body along an arbitrary line will alter the stress. This fact is problematic for many stress measurement techniques, but is exploited by the present method. If we have an ideal cutting process, the inherent strain in each piece of the original body will not be altered by the process. Sectioning of the body changes the distribution of residual stress, but not that of inherent strain. By measuring the stress change when the body is sectioned, the inherent strain can be determined. Further, it need not be assumed that residual stress is entirely relieved by the cutting process in applying this method.

Assuming that the material behavior of the body is linear elastic, we seek a relation between the stress change due to a cutting process,  $\underline{\sigma}$ , and the inherent strain field within the body,  $\underline{\epsilon}^*$ . Representing this relation in tensor notation, we have:

$$\underline{\sigma} = \underline{f}(\underline{\epsilon}^*). \quad [1]$$

Note that  $\underline{\sigma}$  and  $\underline{\epsilon}^*$  are second order tensor functions of the spatial coordinates, so that  $\underline{f}(\bullet)$  is a second order tensor-valued function, also dependent on spatial coordinates.  $\underline{f}(\bullet)$  represents a rather complex set of operations required to solve for stress given the distribution of inherent strain.

Inherent strain enters the elasticity problem through the constitutive relation for an elastic material

$$\underline{\sigma} = \underline{\underline{C}} \bullet (\underline{\varepsilon} - \underline{\varepsilon}^*). \quad [2]$$

where

$$\begin{aligned} \underline{\sigma} &= \text{stress} \\ \underline{\varepsilon} &= \text{total strain} \\ \underline{\varepsilon}^* &= \text{inherent strain} \\ \underline{\underline{C}} &= \text{elastic constitutive tensor} \end{aligned}$$

The total strain field must be found so that equilibrium is satisfied (i.e.,  $\nabla \bullet \underline{\sigma} = 0$ ) in the geometry of interest. In view of [2], the function  $\underline{f}(\bullet)$  could be called the elastic response function of the body due to inherent strain. The solution of [1] can be readily pursued for some specific definition of  $\underline{\varepsilon}^*$ . Finding  $\underline{f}(\bullet)$  in the case of an unknown  $\underline{\varepsilon}^*$  is called for here, since we wish to find the inherent strain which causes  $\underline{\sigma}$ , requiring inversion of [1].

Several approaches to this problem might be employed; however, we will proceed as follows. First, a common set of basis functions for  $\underline{\sigma}$  and  $\underline{\varepsilon}^*$  is adopted. We choose the familiar node points, elements, and linear interpolation functions of finite element analysis (FEA). This is tantamount to assuming that inherent strain and stress are interpolated linearly within several subspaces (elements) within the space of the problem. At the nodes, stress will be determined experimentally, and inherent strain components will be defined. Within the elements, each component of inherent strain is interpolated linearly from the nodal values. As with FEA, the basis functions chosen are not complete, but provide an approximation to  $\underline{\varepsilon}^*$  within the space of the problem.

Some cumbersome notation can be avoided if we adopt a vectorization of  $\underline{\sigma}$ ,  $\underline{\varepsilon}^*$  and  $\underline{f}(\bullet)$ , that is, we will assume that at each interpolation node point we have a definition for each component of  $\underline{\sigma}$ ,  $\underline{\varepsilon}^*$ , and  $\underline{f}(\bullet)$ . If all these components are assembled in a specified but arbitrary order, each may be referred to by only a single index. The assembled vectors of stress, inherent strain, and elastic response are denoted  $\sigma$  and  $\varepsilon^*$ , and  $f(\bullet)$ . In the following then,  $\varepsilon_i^*$  refers to a specified component of  $\underline{\varepsilon}^*$  at a specified node and similarly for  $\sigma_i$ , and  $f_i(\bullet)$ . Further,  $N_i$  refers to a specific interpolation function for each specific component (even though all components are interpolated with the same functions at a given node).

Having chosen a set of basis functions and nodes, we re-write  $\varepsilon^*$  as a sum of nodal values and basis functions

$$\varepsilon^* = \sum_i \varepsilon_i^* N_i \quad [3]$$

Similarly, we can rewrite  $\sigma$  and  $f(\bullet)$

$$\begin{aligned} \sigma &= \sum_i \sigma_i N_i \\ f &= \sum_i f_i N_i. \end{aligned}$$

Since  $f(\varepsilon^*)$  can be defined for any arbitrary  $\varepsilon^*$ , we find it for each  $\varepsilon_i^* N_i$  with  $\varepsilon_i^* = 1$ , and define

$$M_{ij} = f_i(\varepsilon^* = \varepsilon_j^* N_j \big|_{\varepsilon_{j \neq 1}}) \quad [4]$$

Note that  $M_{ij}$  needs to be derived from the equilibrium

equations for the geometry and sectioning process of interest. Finally, we can re-write [1] as

$$\sigma_i = \sum_j M_{ij} \varepsilon_j^*. \quad [5]$$

Here, we have used the fact that each solution  $f(\bullet)$  is itself in equilibrium. Therefore, any linear combination of such solutions will also be in equilibrium according to the principle of superposition.

Now, the complex problem presented by the inversion of [1] is reduced to inversion of the linear system represented by [5]. The matrix  $M_{ij}$  can be interpreted as having columns which represent the change in stress resulting from the sectioning operation of interest when a single inherent strain degree of freedom (DOF) is equal to unity. Each DOF represents a particular component of  $\underline{\varepsilon}^*$  at a particular nodal position. Filling the columns of  $M_{ij}$  for all degrees of freedom,  $\varepsilon_j^*$ , is clearly a job for the computer, and can be accomplished by a general purpose finite element code.

Since we will use the finite element method, which will have its own associated mesh, we will refer to the mesh used to interpolate inherent strain as the background mesh (BGM). We use the term background mesh to avoid confusion with the actual FEA mesh used in the computations. Linear displacement elements are employed in the FEA calculation so that only a constant strain field can be represented exactly within each element. Since the BGM imposes a linear strain field, several linear displacement elements need to be used within each background element. For our purposes, the FEA mesh and the BGM will never be the same.

Formation of the matrix  $M_{ij}$ , or simply  $\mathbf{M}$ , is relatively straight forward using the finite element method. Since each inherent strain DOF is imposed on the same mesh, assembly and factorization of the global stiffness matrix is done only once. Each DOF is then handled as a separate load case in the linear analysis. Post-processing is done to represent  $\mathbf{M}$  in a way that can be imported into a matrix analysis package (e.g., MATLAB) to solve [5].

Since the values of  $\sigma_i$  are determined experimentally, and  $\mathbf{M}$  is formed from repetitive calculation, it is left to solve [5] for the values of  $\varepsilon_j^*$ . This can be accomplished if the number of stress components is equal to or greater than the number of unknown inherent strain components, and if  $\mathbf{M}$  is non-singular. If there are more experimentally determined stresses than unknown inherent strains, a least-squares approach can be used to solve the system with minimized error. Singularities in  $\mathbf{M}$  arise if there is some inherent strain field which produces no stress. Such a strain field will satisfy the compatibility relations of elasticity.

The method of inherent strain is married to the finite element method in that only certain stress and strain fields can be represented exactly, and therefore singular modes in [5] can be identified and removed. As illustrated by H. Reissner (1931), there are infinitely many possible strain fields which satisfy the compatibility relations. Each of these fields will result in zero stress, and therefore cause a singularity in [1]. However, only certain of these will cause zero stress in the

finite-element-approximated system [5]. By considering the type of finite elements used and the type of interpolation used for inherent strain, such singular modes can be identified and suppressed.

Modes which should cause zero stress, but which do not do so because of the inexact nature of the FEA approximation, will make the system [5] ill-conditioned, but not singular. The solution for inherent strain will therefore include some inherent strain field which causes only small stress at points of the BGM. Since our interest is mainly in reproducing stress, and not in the absolute form of inherent strain, such low order modes present in [5] are not of concern. If the inherent strain field were important, it might be possible to apply modal analysis to [5] and specifically eliminate lower-order eigenmodes, but such an approach has not been pursued here. It is interesting to note that refinement of the FEA mesh used in the solution for inherent strain improves the quality of any stress solution, and so serves to further ill-condition the system.

Restricting ourselves for the time being to plane-stress elasticity, we can investigate the form of zero-stress modes for the implementation of the inherent strain method described above. We have assumed linear strain interpolation and linear displacement finite elements. The compatibility condition for plane stress is:

$$\epsilon_{11,22} + \epsilon_{22,11} = \epsilon_{12,12} \quad [6]$$

(Note: Engineering shear strain is assumed throughout this paper.) Any inherent strain field which satisfies this relation will create stress-free deformation. Constant and linear functions of any of the strain components will satisfy [6]. Also, the following strain fields will also satisfy [6] and so give rise to stress free deformation in an unrestrained body in plane stress:

$$\epsilon_{11} = yf_1(x) + g_1(x) + c_1 \quad [7]$$

$$\epsilon_{22} = xf_2(y) + g_2(y) + c_2 \quad [8]$$

$$\epsilon_{12} = f_3(x) + g_3(y) + c_3 \quad [9]$$

where,  $f_i(\bullet)$  and  $g_i(\bullet)$  are arbitrary functions, and  $c_i$  are arbitrary constants. These three fields are the only ones which can exactly produce zero stress in our implementation of the inherent strain method. They can be suppressed by setting certain inherent strain degrees of freedom to be zero in the system. Suppression of modes contained in [7] can be accomplished by setting nodal values of  $\epsilon_{11}^*$  to be zero along two lines of  $y = \text{constant}$  within the background mesh. Similarly, modes contained in [8] can be suppressed by setting nodal values of  $\epsilon_{22}^*$  to be zero along two lines of  $x = \text{constant}$  within the BGM. Finally, modes contained in [9] can be suppressed by setting  $\epsilon_{12}^*$  to be zero along one line of  $y = \text{constant}$  and along one line of  $x = \text{constant}$ .

The inherent strain method can be especially valuable if some knowledge about the distribution of inherent strain is known. For instance, in the case of weld residual stress it can be assumed the inherent strain lies in the vicinity of the weld-line. For shot-peening residual stress on a flat plate, the inherent strain must lie in a shallow surface layer. For residual

stress in a long cylindrical ingot due to quenching, the inherent strain away from the ends may be independent of axial and angular coordinates depending only on radial position (Ueda, 1986). The more that is known about the inherent strain field, the easier the method is to employ.

### **Application of the inherent strain method to a long welded joint**

Of particular interest here is the determination of through-thickness residual stress in a large multi-pass steel weld. If the joint is long and welded continuously, several assumptions can be made about the distribution of inherent strain in the welded joint (Ueda, 1989). As mentioned above, inherent strain will only exist in a region near the weldline. If welding is performed in a continuous fashion, each plane of material transverse to the weldline undergoes nearly the same thermal history. In other words, the thermal history experienced by an element of material during this type of welding is independent of the position along the weld. Inherent strain resulting from welding is a combination of thermal and plastic strain. Thermal strains result from heating and cooling, and plastic strains result when the material surrounding the weld bead restrains thermal straining. If the plate is restrained equally along its length, then the process of welding gives rise to inherent strain which is independent of position along the weld line. It also can be assumed that residual stress in continuous welds is symmetric about the transverse weld direction at the middle of the weld length. This allows elimination of shear components of inherent strain involving the welding direction (e.g., if the weldline corresponds to the  $z$ -direction,  $\epsilon_{13}^* = \epsilon_{23}^* = 0$ ), as they would cause asymmetrical stresses to arise.

### **MODEL PROBLEM TO ILLUSTRATE METHOD**

To illustrate the inherent strain method for determining residual stress in a long welded joint, we will perform a numerical experiment. Functional forms of each inherent strain component are assumed. The finite element method is used to predict the stress distribution arising from the inherent strain. A piecewise-linear distribution of inherent strain is then found which approximates the original inherent strain field from "measured" stress. Finally, stress is determined in regions of the original body where no measurements could be made.

### **Definition of geometry and assumed inherent strain distribution**

The body in which inherent strain is distributed is shown in Fig. 1. This represents a block of material removed from a long welded joint, where the weld runs in the  $z$ -direction (the coordinate system referred to throughout this paper is shown in Fig. 1). It is assumed that the elastic properties of the material are uniform and given by  $E = 30 \times 10^6$  psi and  $\nu = 0.292$ . Inherent strain is imposed within the shaded area of the block only. The inherent strain is dependent on the  $x$  and  $y$

coordinates and is independent of z, following assumptions about continuous welding.

Several qualities of the mathematical form assumed for the inherent strain were desirable. First, the functions were to be spatially continuous and smooth. Since plastic strains due to welding are thought to exist only within two thicknesses of the weldline, functions should be zero outside that region. Also, we wanted these functions to represent a case of deformational symmetry about the x and y center-planes of the body. (Accordingly, the shear strains are asymmetric while the normal strain components are symmetric.) This means that

$$\begin{aligned}\epsilon_{ij}^*(x',y') &= \epsilon_{ij}^*(-x',y') & (i=j) \\ \epsilon_{ij}^*(x',y') &= \epsilon_{ij}^*(x',-y') & (i=j) \\ \epsilon_{ij}^*(x',y') &= -\epsilon_{ij}^*(-x',y') & (i \neq j) \\ \epsilon_{ij}^*(x',y') &= -\epsilon_{ij}^*(x',-y') & (i \neq j)\end{aligned}\quad [10]$$

where i, j = 1, 2, or 3

and where x' and y' are "central" coordinates:  $\begin{cases} x' = x - 4 \\ y' = y + 0.75 \end{cases}$

Other than these considerations, the choice of functions used to represent the inherent strain was arbitrary and done just for the sake of illustration. Mathematical forms chosen for the inherent strain components are:

$$\begin{aligned}\epsilon_{11}^* &= \epsilon_{22}^* = \epsilon_{33}^* = 0.001 * f(x) * g(y) \\ \epsilon_{12}^* &= 0.001 * u(x) * v(y) \\ \epsilon_{13}^* &= \epsilon_{23}^* = 0\end{aligned}$$

where

$$\begin{aligned}f(x) &= 0.5 * \left[ \cos\left(2\pi \frac{x-2.5}{3.0}\right) - 1 \right] \\ u(x) &= 1.73 \left( 1 - \left| \frac{x-4}{1.5} \right| \right) \sin\left(\pi \frac{x-4}{1.5}\right) \\ g(y) &= 0.5 * \left[ 1 + \cos\left(2\pi \frac{y}{1.5}\right) \right] \\ v(y) &= \cos\left(\pi \frac{y}{1.5}\right)\end{aligned}\quad [11]$$

for

$$x \in [2.5, 5.5]$$

and

$$f = g = u = v = 0$$

for

$$x \notin [2.5, 5.5]$$

These functions are shown graphically in Fig. 2.

### **Solution to model problem by application of the finite element method**

The finite element method is employed to find the stress caused by the inherent strain field represented by equations [11] within the body shown in Fig. 1. A general purpose elastic finite element code was used, and inherent strains were imposed by thermal analysis. Anisotropic thermal expansion coefficients were defined in the model as a function of position. Each coefficient was equal to its corresponding inherent strain (e.g.,  $\alpha_{11} = \epsilon_{11}^*$ ) at a given point in the model.

A unit temperature change was then imposed and the equilibrium solution for residual stress was computed.

Sample distributions of the stress field resulting when the inherent strain is imposed in the block geometry of Fig. 1 are shown in Figs. 3 and 4. These stresses will be used in lieu of experimental measurements when demonstrating the inherent strain method, and so will be referred to as the "experimental stress".

The 3D finite element mesh used in the "experimental" solution was more refined than the one used in execution of the inherent strain method, described below. This is important in that any numerical advantage given to the inherent strain method is minimized, so the inherent strain method will truly approximate the more exact experimental solution. The inherent strain method, as described in this paper, is subject to discretization error from two sources. First, the true inherent strain function is approximated by linear interpolation between points of the background mesh. Secondly, the stresses found are an FEA approximation of the "true" stress solution to the approximated inherent strain field. By having both an inherent strain field and an experimental stress field which cannot be represented exactly on the mesh used in execution of the method, we are more likely to examine all the potential errors in the inherent strain method. We therefore designed more refinement into the FEA mesh used to find the experimental solution so that the method could be fully tested.

Inherent strain was imposed in both the block and slice geometry shown in Fig. 1 using the same mesh layout. The depth of the block is 5.0" while the slice is 0.25". One mesh was generated for the block geometry, and then the z-coordinates multiplied by 0.05 to obtain the mesh for the slice. Accordingly, the nodal layout in the x-y plane for both meshes is equivalent. Some of the nodes on this mesh were coincident in the x-y plane with nodes of the BGM so that experimental stress vectors could be assembled. Experimental stress vectors were assembled from free-surface stress to give results on both the block,  $\sigma_b$ , and on the slice,  $\sigma_s$ .

### **SOLUTION FOR INHERENT STRAIN**

The following method for finding inherent strain with assumptions about continuous welding was presented by Ueda (1985). Two measurements of stress will be performed on this object, corresponding to what would be done in actual experiments. At each point where stress is determined, it is assumed that all three components of surface stress are estimated. First, the difference in stress on the surface  $z = z_{max}$  will be measured when a slice of material is cut from the block, as shown in Fig. 1. To perform this measurement, three element strain gage rosettes would be attached to the free surface  $z = z_{max}$  of the block at nodal points in the inherent strain interpolation mesh. Strain released by removing the slice would be measured. The stress change due to cutting,  $\Delta\sigma_s$ , would then be calculated from plane stress elastic constitutive relations. Secondly, the stress change will be recorded when the slice is cut into small pieces. The pieces, if small enough,

will have no stress in them at all. Thus, the stress change between the slice and the small pieces will be nearly the negative of the total stress in the slice,  $\sigma_s$ . Now that the stress which existed in the slice is known, the stress which existed on the block free surface may be estimated from

$$\sigma_b = \sigma_s - \Delta\sigma_s \quad [12]$$

Two quantities have now been estimated: the stress on the free edge of the block,  $\sigma_b$ , and the stress in the slice  $\sigma_s$ . (The above procedure could be called slice-and-dice.)

Since this is a numerical experiment, we will use the stress solutions for  $\sigma_b$  and  $\sigma_s$  obtained using FEA and described earlier to solve the inherent strain problem.

Ueda (1985) assumes that if the slice is cut thinly enough, stress caused by the inherent strain component normal to the slice will be zero. If this is indeed the case, the problem is reduced to one of plane stress, greatly reducing the complexity of the problem, and the computational burden in formulating  $\mathbf{M}$ . This also de-couples the components within the plane ( $\epsilon_{11}^*$ ,  $\epsilon_{22}^*$  and  $\epsilon_{12}^*$ ) from that out of the plane ( $\epsilon_{33}^*$ ). These two sets of inherent strain components are respectively referred to as the cross-sectional inherent strain and the longitudinal inherent strain by Ueda.

### Cross-sectional inherent strain

Taking the assumption that a thin slice can be modeled in plane stress, a 2D finite element mesh is constructed based on the slice geometry shown in Fig. 1. With the background mesh defined by the strain gage layout described in the last section, degrees of freedom for  $\mathbf{M}$  are also defined. At each point in the BGM, we have a freedom for  $\epsilon_{11}^*$ ,  $\epsilon_{22}^*$  and  $\epsilon_{12}^*$ . Some degrees of freedom, however, need to be eliminated to suppress singularities in  $\mathbf{M}$ . Once the system  $\mathbf{M}$  is formed, as outlined above, the experimental stress in the slice  $\sigma_s$  is then used to solve [5] for the cross sectional inherent strain,  $\epsilon_c^*$ , at the nodes of the BGM.

To solve the model problem, the BGM assumed is rectangular, with nodal spacing  $\Delta x = 0.4$ " and  $\Delta y = 0.25$ ". The mesh points fall within  $x \in [0.2, 7.8]$  and  $y \in [0, -1.5]$ , yielding 140 background nodes (7 in the y-direction by 20 in the x-direction). Note that all elements of the BGM are the same size, except for elements at the ends, where  $\Delta x = 0.2$ " instead of 0.4". The finite element mesh used to construct  $\mathbf{M}$  had four elements for each element of the BGM, except on the ends. All finite elements were the same size,  $\Delta x = 0.2$ " and  $\Delta y = 0.125$ ".

To remove singular modes represented by [7],  $\epsilon_{11}^*$  is taken to be zero at all nodes on  $y = 0.0$  and  $y = -1.5$ ". There are no nodes on  $x = 0$  and  $x = 8.0$  so modes represented by [8] are already suppressed. Modes represented by [9] are suppressed by setting  $\epsilon_{12}^* = 0$  for all nodes on  $y=0$ . The background mesh contains 140 nodes, but instead of 420 DOFs, we have only 360 non-zero components (i.e., we have suppressed 60 DOFs). Therefore, the dimension of  $\mathbf{M}$  is 420 by 360, and least squares is used to solve for the inherent strain.

### Longitudinal inherent strain

Now that  $\epsilon_c^*$  has been estimated on the BGM, these inherent strain components are defined within the block geometry on a 3D FEA mesh, and the equilibrium solution obtained. The stress on the free surface  $z = z_{max}$  is collected at the points of the BGM. This is the stress in the block,  $\sigma_b^c$ , resulting only from the estimate of cross-sectional components of inherent strain. Now, we construct the difference between  $\sigma_b$  and  $\sigma_b^c$  at each point in the BGM

$$\Delta\sigma_b = \sigma_b - \sigma_b^c. \quad [13]$$

This difference is due to the absent longitudinal inherent strain,  $\epsilon_1^*$ . So, a new system  $\mathbf{M}$  is assembled relating  $\epsilon_1^*$  to stress on the free surface of the block, and the system solved for  $\epsilon_1^*$  given  $\Delta\sigma_b$ .

The 3D FEA mesh used to find  $\sigma_b^c$  and to form  $\mathbf{M}$  has the same layout in the x-y plane as the planar mesh used to find  $\epsilon_c^*$ . The layout in the thickness direction consists of five elements. The nodes are spaced in the z-direction in geometric progression such that the ratio of the thickness of the last element to the first is 10:1.

## **RESULTS**

Solving the model problem as described in the previous section, and imposing the resulting approximated inherent strain distribution onto the 3D FEA mesh for the block gives the approximate distribution of residual stress in the block. Scaling this same mesh in the z-direction and imposing the approximate inherent strain gives results for the slice. Note that all components of inherent strain were imposed in the slice geometry, even though we assumed that  $\epsilon_{33}^*$  would cause no stress in the slice in our application of the inherent strain method. We can now compare the results of the inherent strain method with the FEA predicted stress which will be referred to as the "exact" solution.

Results for the stress in the slice are shown in Figs. 5 and 6. In the figures, the inherent strain solution is denoted "IE" and the exact solution "FEA". Agreement between the estimated and exact values of stress is apparent. The error in the approximation on the line  $x=3.8$  is shown in Fig. 7. As might be expected, errors are largest at nodes not coincident with the background mesh. (Nodes coincident with the background mesh are shown with symbols in the figure.) Among values at points on the background mesh, errors are less than 1.5 ksi, or 8% of the maximum measured stress. It should be noted that errors on the line  $x=4.0$  are somewhat larger than those on  $x=3.8$ , since background mesh points do not fall on  $x=4.0$ .

Results for stress in the block are shown in Figs. 8, 9 and 10. Stress results on the free surface, where stress measurements were taken, show agreement which is not quite as good as for the slice. Maximum error in the stresses found by the inherent strain method is 17% of the maximum measured stress on the free surface, and occurs at  $x = 3.8$ ,  $y = -0.75$ . Mid-plane results show more error, especially in the

longitudinal stress,  $\sigma_{33}$ . Maximum error is about 30% of the maximum stress for this component. Since the longitudinal stress was never measured and no stress measurements were done in the vicinity of the block mid-plane, that there is any sort of agreement at all may still be somewhat surprising.

The errors present in the block stress are higher than one would like, especially in the longitudinal stress at the block mid-plane. A likely explanation for larger errors in the longitudinal stress might be that the approximation of the cross-sectional inherent strain is used to predict the longitudinal inherent strain. So, errors in the cross-sectional inherent strain propagate into the prediction of longitudinal inherent strain, causing larger errors in estimated longitudinal stress. Perhaps use of the inherent strain prediction of slice stress to find  $\sigma_b$  in [12] would lessen this error, but that has not been investigated. Another explanation might be that the longitudinal inherent strain actually causes stress in the slice, and the cross-sectional and longitudinal components cannot be uncoupled without errors. Figure 11 shows the stress produced on the free surface of the slice when only the approximate longitudinal inherent strain is imposed. Values here are as much as 10% of the stresses present in the slice shown in Fig. 5.

## DISCUSSION

The method proposed by Ueda (1975) to measure three-dimensional residual stress using a hybrid experimental-analytical approach has been shown to provide reasonable predictions of residual stress for the model problem considered here. However, noticeable errors are present in the method, the source of which needs to be more thoroughly investigated. Coupling of longitudinal and cross-sectional inherent strains could be investigated by modeling the slice as three-dimensional. The use of other basis functions could also be studied, perhaps finding a set which excludes singular modes of inherent strain. Also, the type and number of finite elements used to solve the inherent strain problem could be optimized. Despite its shortcomings, this approach holds promise and provides reasonably accurate results.

More importantly, this is one of the few methods available for finding subsurface three-dimensional residual stresses. The method proposed previously by Norton and Rosenthal (1945) could have also been used to approach this problem. This method unfortunately makes use of a questionable assumption. Applying their assumptions to our geometry, we would reason that if the slice in Fig. 1 is removed from the middle of the block, the distribution of released stress would be a linear function of depth from the surface (i.e., linear in  $y$ ). We can check this assumption with our "exact" FEA solution. Subtracting the stress in the mid-plane of the slice from the stress in the mid-plane of the block yields the stress released when a slice is removed from the center of the block. This quantity is plotted in Fig. 12 and is clearly non-linear. Ueda's method provides a way to bypass the overly simplified

assumptions of Norton and Rosenthal in solving for residual stress.

The inherent strain method is attractive in that it provides a whole field approach to the prediction of residual stress. Many methods of residual stress estimation provide results on a single plane or at a single point within a component. Such information is useful for fatigue and linearly elastic fracture mechanics analyses. However, if elastic-plastic fracture analysis is to be pursued, having stress on a single plane does not allow for generalized redistribution of residual stress caused by plasticity. Such redistribution could only be studied if the entire residual stress field were known. Use of the inherent strain method would provide information necessary to perform an elastic-plastic fracture assessment including residual stress relaxation due to plastic flow.

Considering that an inherent strain field is the outcome of any mechanical operation, finding inherent strain provides a way to characterize manufacturing processes. Mechanical processes have been characterized to a large degree by the residual stresses they produce. This has been done for a number of operations (e.g., grinding, shot-peening, welding, and induction hardening). But, since residual stress depends on the geometry of the part, inherent strain may provide a better basis for comparison of similar processes.

Although solution for the distribution of residual stress within a body is an attractive feature of the inherent strain method, it also mandates the need for a large amount of experimental measurements. (In the solution to the model problem, 140 three-element strain rosettes would have been employed, each being measured twice.) If residual stress is needed only within a small region of interest within the body, it would be interesting to investigate if this method could be localized, thereby reducing the number of experimental measurements required for stress prediction. Such an approach could provide the benefit of estimating three-dimensional residual stress in geometries other than those in which stress is measured, while not requiring as much experimental effort.

## SUMMARY

The inherent strain method, which allows the prediction of residual stress within a body from which a sample has been removed, was outlined and then implemented to solve a model problem. Application of the method to the model problem revealed that reasonable estimates of residual stress are obtained. Nevertheless, errors were present in the estimates, and possible sources of these errors were postulated. Lastly, benefits of the method and obstacles to its application were discussed. The inherent strain method remains one of the only methods for determination of three-dimensional subsurface residual stress.

## ACKNOWLEDGMENTS

Funds for the support of this study have been allocated by the NASA-Ames Research Center, Moffett Field, California, under Interchange No. NCA2-767.

**REFERENCES**

D. Rosenthal and J. T. Norton, 1945, "A Method of Measuring Triaxial Residual Stresses in Plates," *Welding J.*, Vol. 24, pp. 295s-307s.

H. Reissner, 1931, "Eigenspannungen und Eigenspannungsquellen," *Zeitschrift für Angewandte Mathematik und Mechanik*, Vol. 11 n1, pp. 1-8.

Y. Ueda, K. Fukuda, K. Nakacho and S. Endo, 1975, "A New Measuring Method of Residual Stresses With The Aid of Finite Element Method And Reliability of Estimated Values," *Trans. Japan Welding Research Institute*, Vol. 4 n2, pp. 123-131.

Y. Ueda, Y. C. Kim and A. Umekuni, 1985, "Measuring Theory of Three-Dimensional Residual Stresses Using a Thinly Sliced Plate Perpendicular to Welded Line," *Trans. JWRI*, Vol. 14 n2, pp. 151-157.

Y. Ueda, K. Fukuda and Y. C. Kim, 1986, "New Measuring Method of Axisymmetric Three-Dimensional Residual Stresses Using Inherent Strains as Parameters," *J. Engineering Materials and Technology*, Vol. 108 n4, pp. 328-334.

Y. Ueda and K. Fukuda, 1989, "New Measuring Method Of Three-Dimensional Residual Stresses In Long Welded Joints Using Inherent Strains As Parameters -  $L_z$  Method," *J. Engineering Materials and Technology*, Vol. 111 n1, pp. 1-8.

**FIGURES**

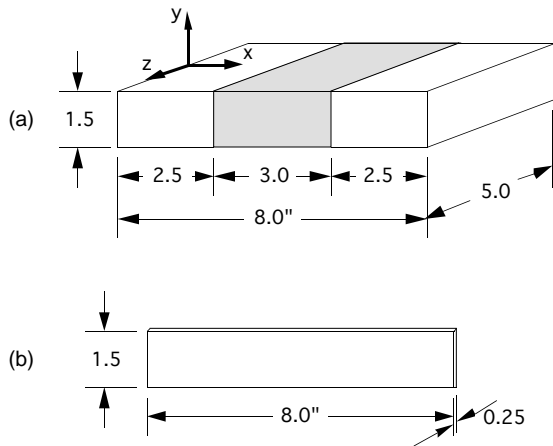


FIG. 1 - (a) BLOCK AND (b) SLICE REMOVED FROM THE END OF THE BLOCK.

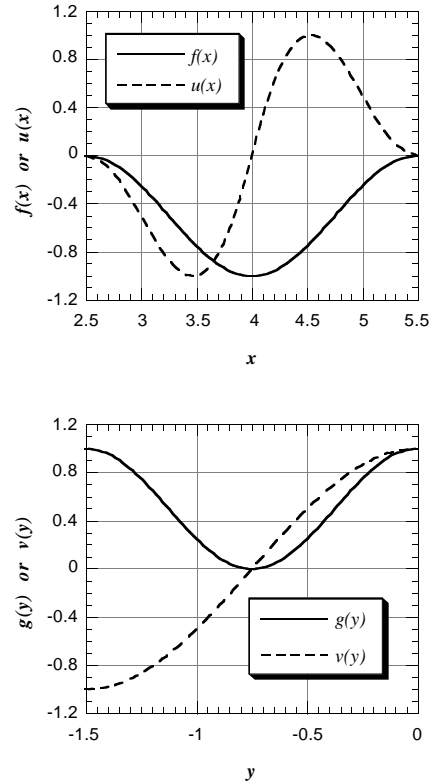
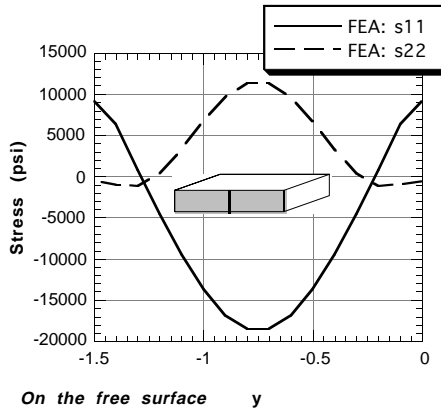
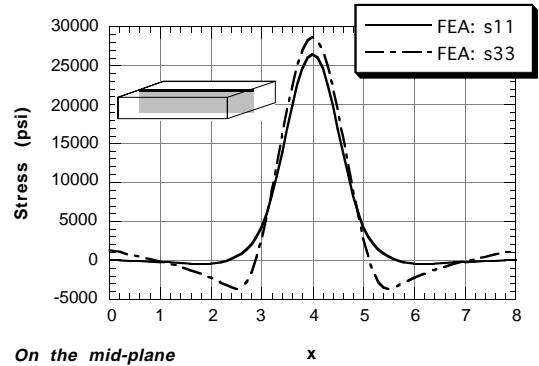


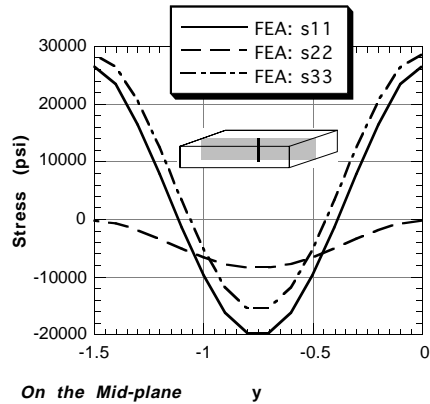
FIG. 2 - FUNCTIONS USED TO DEFINE A DISTRIBUTION OF INHERENT STRAIN.



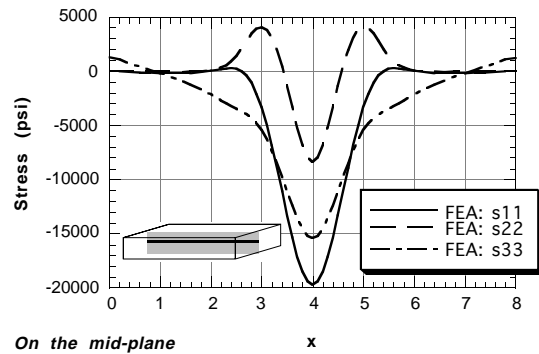
On the free surface  $y$



On the mid-plane  $x$



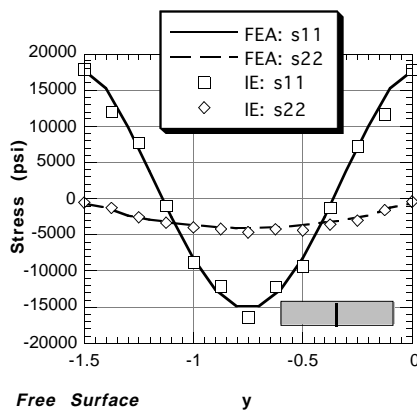
On the Mid-plane  $y$



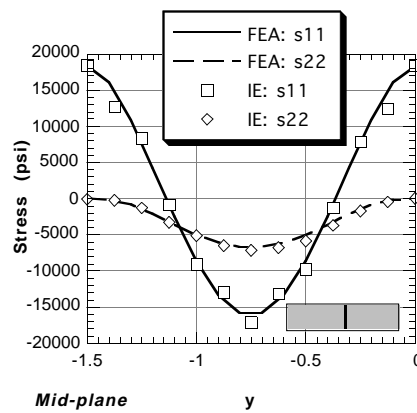
On the mid-plane  $x$

FIG. 3 - STRESS IN THE BLOCK RESULTING FROM INHERENT STRAIN ON THE LINE  $X = 4.0$  ON THE FREE SURFACE,  $Z = Z_{MAX}$ , AND THE MID-PLANE OF  $Z$  SYMMETRY,  $Z = 0$ .

FIG. 4 - STRESS IN THE BLOCK RESULTING FROM INHERENT STRAIN ON THE MID-PLANE,  $Z=0$ , ON THE LINES  $Y = 0$  AND  $Y=-0.75$ .



Free Surface  $y$



Mid-plane  $y$

FIG. 5 - EXACT (FEA) AND APPROXIMATE (IE) STRESS IN THE SLICE ON LINE  $X=3.8$  ON THE FREE SURFACE,  $Z = Z_{MAX}$ , AND THE MID-PLANE,  $Z = 0$ .

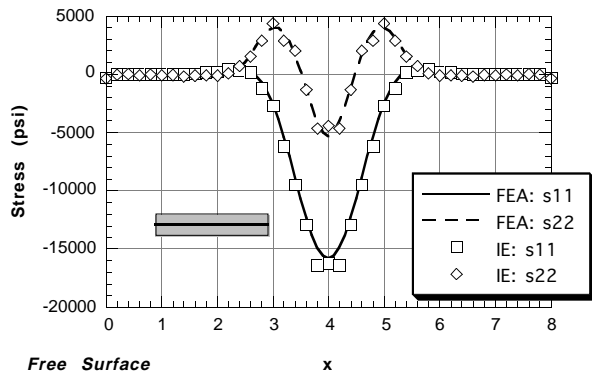


FIG. 6 - EXACT (FEA) AND APPROXIMATE (IE) STRESS IN THE SLICE ON THE LINE  $Y = -0.75$  ON THE FREE SURFACE,  $Z = 0$ .

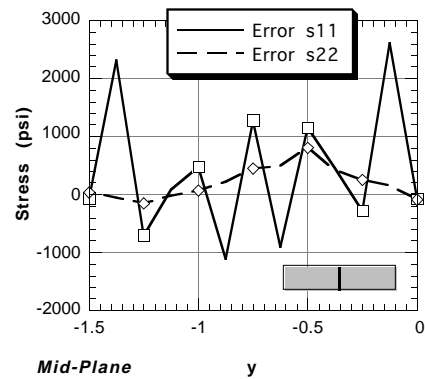
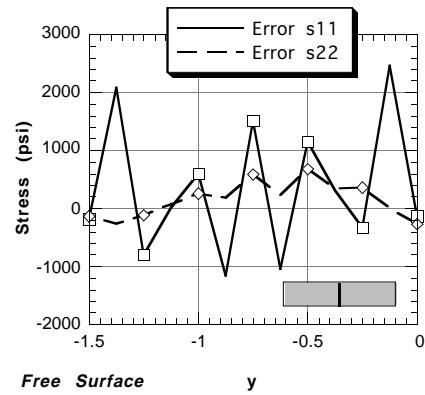


FIG. 7 - ERROR IN APPROXIMATION OF STRESS SHOWN IN FIG. 5. POINTS WITH SYMBOLS ( $\square$  AND  $\diamond$ ) REPRESENT POINTS ON THE BACKGROUND MESH.

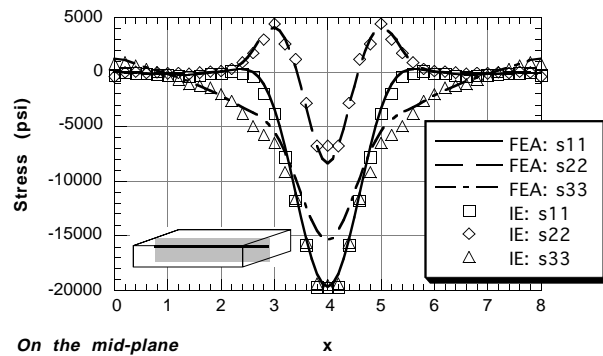
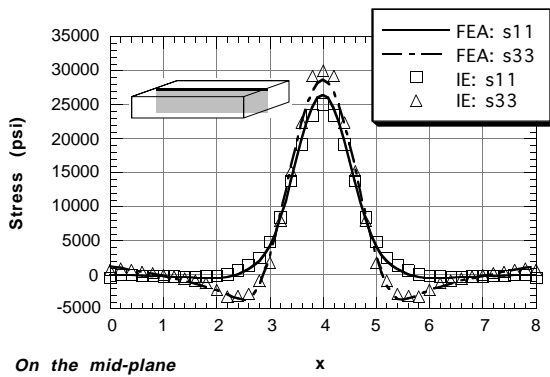


FIG. 8 - EXACT (FEA) AND APPROXIMATE (IE) STRESS IN THE BLOCK ON THE MID-PLANE,  $Z=0$ , ON THE LINES  $Y = 0$  AND  $Y=-0.75$ .

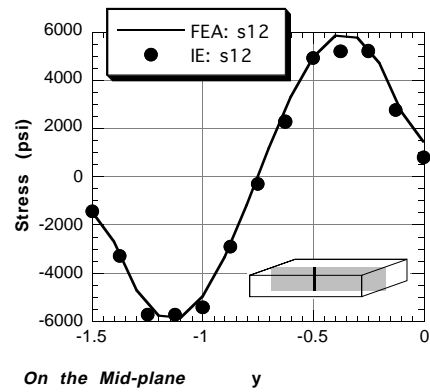
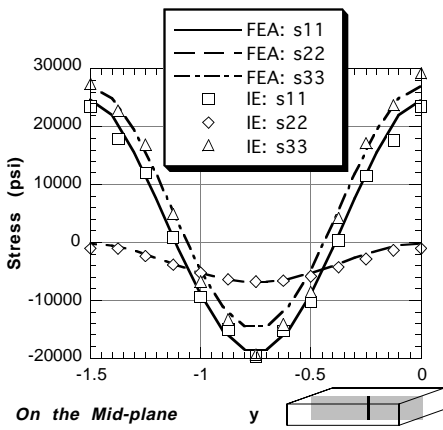
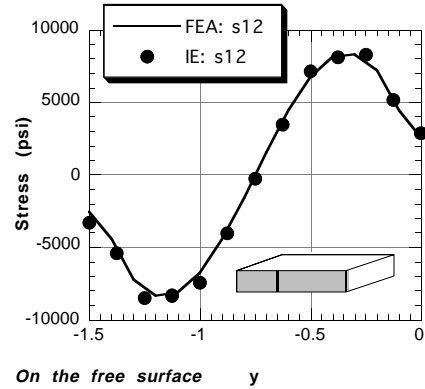
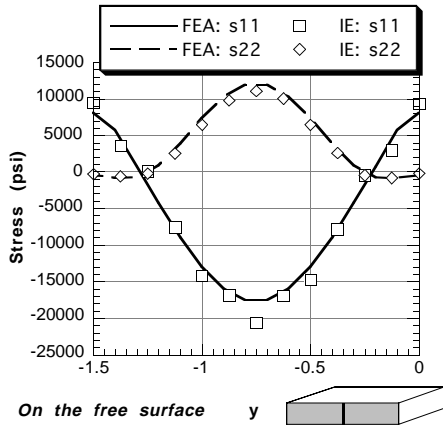


FIG. 9 - EXACT (FEA) AND APPROXIMATE (IE) STRESS IN THE BLOCK ON THE LINE  $X = 3.8$  ON THE FREE SURFACE,  $Z = 0$ , AND MID-PLANE,  $Z = Z_{MAX}$ .

FIG. 10 - EXACT (FEA) AND APPROXIMATE (IE) SHEAR STRESS IN THE BLOCK ON THE LINE  $X = 3.4$  ON THE FREE SURFACE,  $Z = 0$ , AND MID-PLANE,  $Z = Z_{MAX}$ .

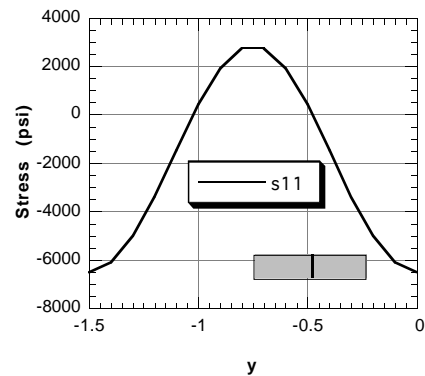
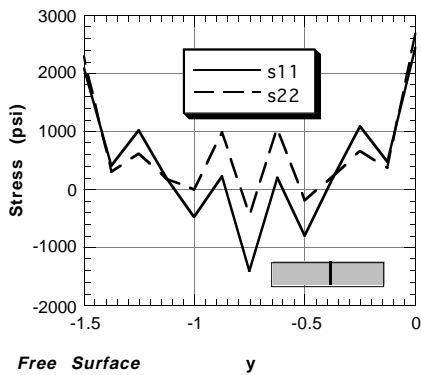


FIG. 11 - STRESS ON THE FREE SURFACE OF THE SLICE DUE ONLY TO LONGITUDINAL INHERENT STRAIN ON THE LINE  $X=3.8$ .

FIG. 12 - STRESS RELEASED IF A SLICE WAS REMOVED FROM THE BLOCK MID-PLANE,  $Z = 0$ , ON THE LINE  $X = 4.0$ .